Synthesis, Redox Properties, and EPR Spectroscopy of Manganese(III) Complexes of the Ligand *N,N*-Bis(2-hydroxybenzyl)-*N'*-2-hydroxybenzylidene-1,2-diaminoethane: Formation of Mononuclear, Dinuclear, and Even Higher Nuclearity Complexes

Heimo Schmitt,[a] Reiner Lomoth,[b] Ann Magnuson,[c] Jonathan Park,[c] Jacob Fryxelius,[a] Mikael Kritikos,[d] Jerker Mårtensson,[e] Leif Hammarström,[b] Licheng Sun,[a] and Björn Åkermark*[a]

Abstract: The synthesis and characterization of the title trisphenolate ligand are described. From its reaction with manganese(III) three complexes were isolated. The crystal structures revealed one pentacoordinate monomer and two similar dimers with different solvents of crystallization. In the dimers the metal ions are hexacoordinate and connected through bridging of two phenolates. A combination of electrochemistry and EPR spectroscopy showed that, in acetonitrile, the isolated batches were all identical and mainly monomeric, indicating that the mononuclear complex is in equilibrium with the dimer and perhaps also with complexes of higher nuclearity, as suggested by the detection of both the trimer and the tetramer by electrospray ionization mass spectrometry (ESI-MS). The successful use of the monomer batch as an epoxidation catalyst indicated that a high-valent manganese – oxo species can be formed, although it is probably short-lived. This is also suggested by EPR studies of the species formed by electrochemical oxidation of the complex. Upon one-electron oxidation, a manganese(IV) species was formed, which was at least partly converted to another species containing a phenoxy radical.

Keywords: EPR spectroscopy · manganese · redox chemistry · structure elucidation

Introduction

In oxygenic photosynthesis, conversion of carbon dioxide into biomass by light energy with electrons derived from water is initiated by excitation of chlorophyll P_{680} at the reaction center, followed by transfer of one electron to the acceptor system. The oxidized chlorophyll, P_{680}^+, is rapidly reduced back to P_{680} by an electron from the water oxidation center (WOC).[1–5] This consists of a tyrosine residue, Tyrosine$_Z$, and a cluster of four manganese ions which functions as a storage device for up to four oxidizing equivalents. Neither the detailed water oxidation mechanism nor the structure of the manganese cluster is known but clearly the manganese ions are oxidized in several steps in the catalytic cycle.[4, 5] It is also very likely that high-valent manganese complexes are involved (for extensive discussion and earlier references, see references [5–7]).

One suggested mechanism, based on quantum-chemical calculations, involves addition of water to a high-valent Mn – oxo complex.[6] Recently, a dimer consisting of high-valent manganese coordinated to terpyridine was shown to catalyze oxidation of water by oxone.[7] Since oxone is used as oxidant, manganese(V)– or manganese(IV)–oxo complexes are most certainly intermediates in the reaction. High-valent mononuclear manganese–oxo complexes with phenolic ligands are also intermediates in epoxidation of alkenes.[8–12] No such complexes have been isolated but a few high-valent oxo complexes with amide ligands have been characterized.[13, 14] However, there are some recent examples of manganese(IV,IV) dimers with one or two phenolic ligands per manganese atom.[15, 16] Some stable monomeric manganese(IV) complexes

[a] Prof. Dr. B. Åkermark, Dr. H. Schmitt, J. Fryxelius, Dr. L. Sun
Department of Organic Chemistry
Stockholm University (Sweden)
Fax: (+46)8-154908
E-mail: bjorn.akermark@organ.su.se

[b] Dr. R. Lomoth, Dr. L. Hammarström
Department of Physical Chemistry
Uppsala University (Sweden)

[c] Dr. A. Magnuson, J. Park
Department of Biochemistry
Lund University (Sweden)

[d] Dr. M. Kritikos
Department of Structural Chemistry
Stockholm University (Sweden)

[e] Dr. J. Mårtensson
Department of Organic Chemistry
Chalmers Technical University, Göteborg (Sweden)

Supporting information for this article is available on the WWW under http://www.chemeurj.org or from the author.

with one phenolic ligand are also known.[17, 18, 19] To see if phenolic ligands could stablize manganese(v) – oxo species, we aimed to prepare a manganese(III) – trisphenoxy complex and to investigate whether it could be transformed into a high-valent oxo complex. As a first attempt, we have synthesized the trisphenolic ligand N,N,N'-tris(2-hydroxybenzyl)-1,2-diaminoethane (1), which reacts with manganese(III) acetate to give a complex (2), in which the secondary amine of the ligand has been oxidized to imine by excess manganese(III). Two related dinuclear complexes, 3a and 3b, have also been isolated.

Results and Discussion

Synthesis: The preparation of the complex 2 was straightforward. The condensation of 2-hydroxybenzaldehyde and 1,2-diaminoethane, followed by reduction by borohydride, gave N,N'-2,2'-bis(2-hydroxybenzyl)-1,2-diaminoethane. This was then condensed with 2-hydroxybenzaldehyde and the cyclic product was reduced by borohydride to give N,N,N'-tris(2-hydroxybenzyl)-1,2-diaminoethane (1) (Scheme 1).

On reaction with manganese(III) perchlorate in the presence of sodium acetate, 1 gave the complex 2 in fair yield. In the process of complex formation, the secondary amine function of the ligand was oxidized to imine. This type of dehydrogenation process has been observed in some related dimeric manganese complexes as well as in a monomeric cobalt tetrahydrosalen complex.[16, 20] Crystallization of the complex gave a monomer 2 and two related dimers 3a and 3b, depending on the conditions. This suggests that the monomer and the dimers have similar energies and could be in equilibrium in solution [Eq. (1)]. This is supported by the electrospray ionization mass spectrum of the crude precipitate from addition of manganese(III) to the ligand 1 (Figure 1), which shows strong peaks for the protonated monomer 2 at m/z 429.8 and the solvent-free dimer 3 at m/z 858.1. Cyclic voltammetry has shown, in a moderately coordinating solvent such as acetonitrile, that 2 is the dominant species.

(1)

2   **3**
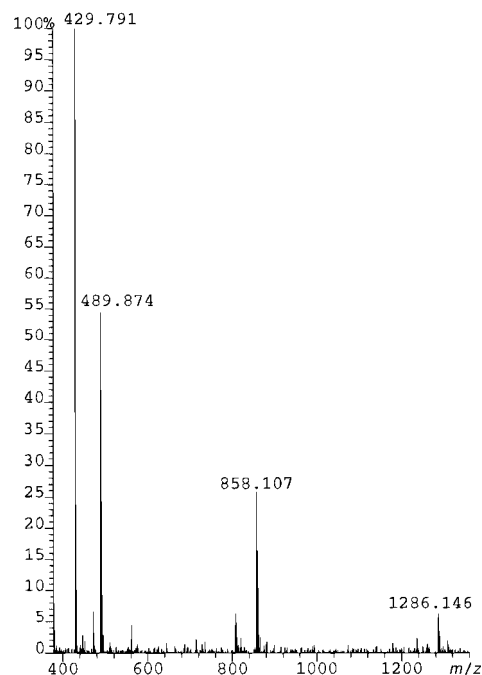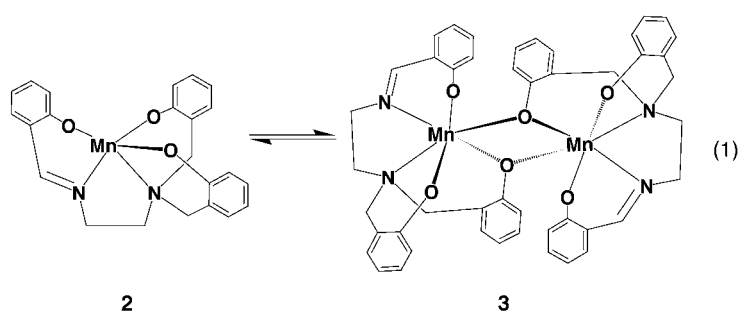
Figure 1. Mass spectrum of the crude precipitate from the reaction of Mn^{III} with the ligand **1**.

According to susceptibility measurements (for which we thank Prof. J. J. Girerd), crude preparations of 2 and 3a also contain a third species, which seems to be a trimer. It is therefore possible that the monomer – dimer equilibrium also includes higher species such as trimer and even tetramer, as suggested by the appearance in the mass spectrum of a substantial peak from the trimer at m/z 1286.1 and a small peak from the tetramer at m/z 1714.7 in the crude product from preparation of 3b (Figure 1).

Solid-state structures: The structures of 2 and 3 in the solid state were determined by single-crystal X-ray crystallography (Table 1).

Crystal structure of 2: The unit cell contains four units of 2, one
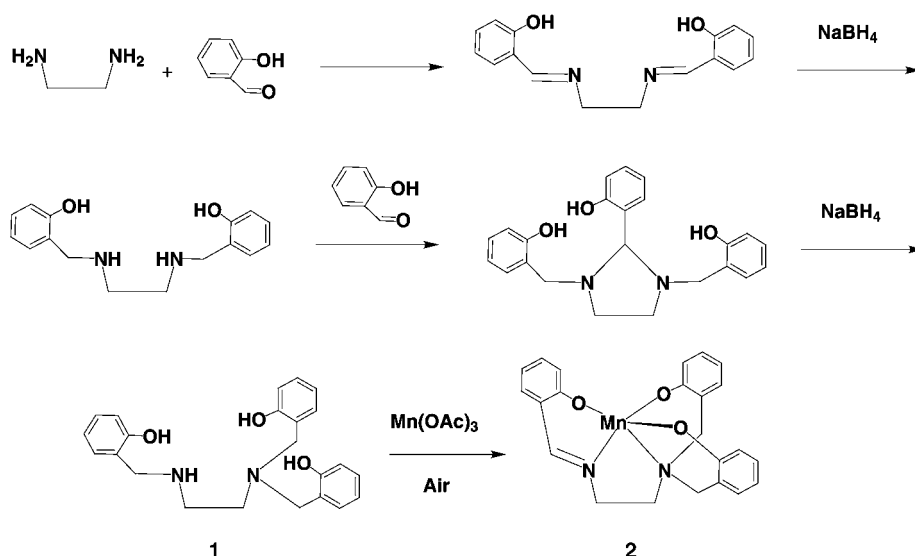
Scheme 1. Synthesis of manganese(III) – N,N-bis(2-hydroxybenzyl)-N'-2-hydroxybenzylidene-1,2-diaminoethane complexes **2**.

Table 1. Selected crystal data for **2**, **3a**, and **3b**.

	2	**3a**	**3b**
empirical formula	$C_{23}H_{21}MnN_2O_3$	$C_{48}H_{50}Mn_2O_8N_4$	$C_{47}H_{48}Mn_2O_8N_4Cl_2$
M_r	428.36	920.80	977.69
crystal system	monoclinic	monoclinic	triclinic
space group	$P2_1/n$ (no. 14)	$P2_1/n$ (no. 14)	$P\bar{1}$ (no. 2)
Z	4	2	1
a [Å]	13.648(2)	10.0688(9)	10.133(2)
b [Å]	7.1591(8)	16.767(2)	11.135(2)
c [Å]	19.831(2)	12.670(1)	12.548(2)
α [°]			115.715(19)
β [°]	97.828(13)	98.523(11)	107.11(2)
γ [°]			96.31(2)
V [Å]^3	1919.6(4)	2115.4(3)	1171.8(4)
crystal size [mm^3]	$0.03 \times 0.12 \times 0.22$	$0.09 \times 0.34 \times 0.42$	$0.17 \times 0.17 \times 0.20$
ρ_{calcd} [g cm^{-3}]	1.482(1)	1.446(1)	1.456(1)
temperature [K]	293(1)	110(1)	293(1)
μ (Mo$_{K\alpha}$) [mm^{-1}]	0.716	0.658	0.820
$F(000)$	888.0	960.0	529.0
N(obs), N(par)	1889, 262	2695, 322	1979, 305
R(int)	0.0966	0.0874	0.1271
S(goodness of fit)	0.770	0.984	0.752
$R1$, $wR2$, ($I > 2\sigma(I)$)	0.0362, 0.0605	0.0387, 0.0817	0.0687, 0.1556
$\Delta\rho_{max}$, $\Delta\rho_{min}$ [e Å^3]	0.27, − 0.39	0.68, − 1.14	0.62, − 0.92

of which constitutes the asymmetric unit. Selected bond lengths and angles are given in Table 2. In the complex (Figure 2), the central Mn atom is bonded to the three O atoms and to two N atoms of the pentadentate ligand,
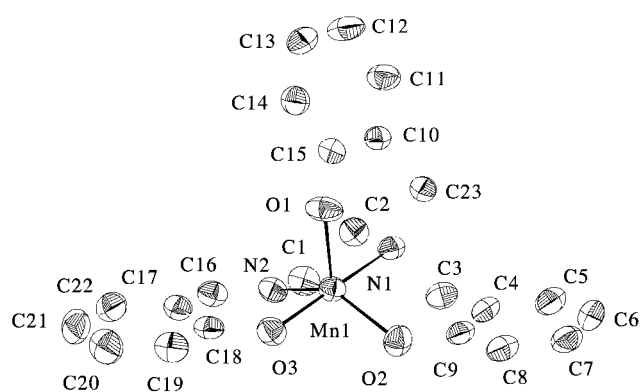
Figure 2. Structure of $C_{23}H_{21}MnN_2O_3$ (**2**) (ORTEP view; ellipsoids at 50 % probability level).

Table 2. Selected bond lengths [Å] and angles [°] for **2**.

Mn1−O1	1.969(2)	O3−C18	1.330(4)
Mn1−O2	1.914(2)	N1−C2	1.500(4)
Mn1−O3	1.863(2)	N1−C3	1.506(4)
Mn1−N1	2.073(2)	N1−C23	1.508(4)
Mn1−N2	2.005(2)	N2−C1	1.462(4)
O1−C15	1.329(4)	N2−C16	1.283(4)
O2−C9	1.340(3)		
O1-Mn1-O2	110.39(9)	Mn1-O1-C15	126.18(19)
O1-Mn1-O3	94.15(10)	Mn1-O2-C9	126.7(2)
O1-Mn1-N1	92.33(9)	Mn1-O3-C18	127.2(2)
O1-Mn1-N2	110.77(10)	Mn1-N1-C2	109.16(17)
O2-Mn1-O3	90.83(9)	Mn1-N1-C3	107.88(17)
O2-Mn1-N1	93.48(9)	Mn1-N1-C23	111.87(16)
O2-Mn1-N2	138.70(10)	Mn1-N2-C1	113.95(18)
O3-Mn1-N1	170.45(9)	Mn1-N2-C16	124.78(19)
O3-Mn1-N2	89.47(10)	N1-Mn1-N2	81.66(9)

exhibiting a very distorted coordination, which is intermediate between a trigonal bipyramid (tbp) and a square pyramid (sp).

The tbp can be regarded as built up from the almost coplanar atoms Mn1, O1, O2 and N2 defining the equatorial plane (the largest deviation of the atoms from this mean plane is 0.03 Å), and by atoms O3 and N1 defining the apical positions. The axial atoms have an N1-Mn1-O3 angle of 170.4°. Alternatively, the structure can be regarded as a distorted sp with O1 as the axial ligand. This interpretation is attractive because of the unusually long Mn−O1 distance, 1.969 Å, and also because it fits with the EPR data (see below). The fivefold coordination geometry adopted may be quantified by using the τ descriptor for five-coordination suggested by Addison et al.[21] This distortion index is defined as $\tau = (\alpha - \beta)/60$. For an ideal C_{4v} sp, $\tau = 0$; for a C_{3v} tbp $\tau = 1$. A τ value of 0.53 supports the observation of a very distorted fivefold coordination. The most frequently encountered coordination geometry of Mn complexes with N_2O_3 donor sets is the slightly distorted sp geometry.

A short C16−N2 distance (1.283 Å) indicates the presence of a C=N imine bond and that the pentadentate ligand has undergone oxidation during the complexation reaction. Most of the other bond lengths are in the same range as in related complexes: the Mn−N bonds are 2.073 – 2.100 Å for the bond to the aliphatic amine nitrogen atom, and the Mn−N=C bonds are 2.005 – 2.188 Å.[16, 22–27] The same is true for the Mn−phenolate bonds, which range from 1.863 to 1.919 Å.[16, 23] The only exception is the long Mn−O1 bond (1.969 Å) mentioned above.

To assess the oxidation state of the Mn atom from the X-ray diffraction structural parameters, bond valence sums were calculated. The analysis, based on the method of O'Keeffe and Brese, gave a reasonable oxidation state of 3.17, somewhat above that found for complex **3a** and the expected value of +3.[28]

Although the solid-state structure of **2** consists of discrete molecules, with a nonbonding Mn···Mn distance of 4.617 Å between neighboring molecules, there is a rather short intermolecular contact (3.323 Å) between O3 and C3^i ($i = 1-x, -y, 2-z$) which could possibly indicate a non-van der Waals contact. In this context, weakly associated monomers of some related pentacoordinate Mn^{III} complexes have been reported, such as [(3,6-(CH$_3$)$_2$salophen)Mn^{III}]PF$_6$ · H$_2$O and Mn(salen)[2-(3-oxobutenyl)phenolate].[29, 30] However, in these compounds the closest intermolecular interaction is between the central Mn atom and a ligand O atom in an adjacent molecule.

Crystal structure of **3a**: The crystal and molecular structures are shown in Figure 3a, and selected bond lengths and angles in Table 3. The unit cell contains two formula units of the centrosymmetric dimeric complex together with two methanol solvent molecules. The CH_3OH molecule is connected to

Table 3. Selected bond lengths [Å] and angles [°] for **3a**.[a]

Mn1−Mn1^i	3.3168(8)	C4−C9	1.403(4)
Mn1−O2	1.884(2)	C5−C6	1.379(5)
Mn1−O1	1.907(2)	C6−C7	1.382(5)
Mn1−O3^i	1.919(2)	C7−C8	1.386(4)
Mn1−N1	2.100(2)	C8−C9	1.400(4)
Mn1−N2	2.188(3)	C10−C15	1.392(4)
Mn1−O3	2.264(2)	C10−C11	1.397(4)
O2−C9	1.352(3)	C10−C23	1.509(4)
O1−C18	1.339(3)	C11−C12	1.390(5)
O3−C15^i	1.366(3)	C12−C13	1.380(5)
O4−C24	1.401(5)	C13−C14^i	1.392(4)
N1−C3	1.499(4)	C15−C14^i	1.397(4)
N1−C1	1.504(4)	C16−C17	1.446(4)
N1−C23	1.508(4)	C17−C22	1.405(4)
N2−C16	1.277(4)	C17−C18	1.419(4)
N2−C2	1.466(4)	C18−C19	1.403(4)
C1−C2	1.527(4)	C19−C20	1.382(4)
C3−C4	1.504(4)	C20−C21	1.389(5)
C4−C5	1.401(4)	C21−C22	1.382(5)
O2-Mn1-O1	89.44(9)	C18-O1-Mn1	127.3(2)
O2-Mn1-O3^i	166.36(9)	C9-O2-Mn1	129.2(2)
O1-Mn1-O3^i	93.51(9)	C15^i-O3-Mn1^i	118.5(2)
O2-Mn1-N1	88.95(9)	C15^i-O3-Mn1	126.9(2)
O1-Mn1-N1	164.22(9)	Mn1-O3-Mn1^i	104.64(8)
O3^i-Mn1-N1	91.74(9)	C3-N1-C1	109.2(2)
O2-Mn1-N2	98.10(10)	C3-N1-C23	106.1(2)
O1-Mn1-N2	86.16(9)	C1-N1-C23	111.2(2)
O3^i-Mn1-N2	95.38(9)	C3-N1-Mn1	110.3(2)
N1-Mn1-N2	78.53(9)	C1-N1-Mn1	107.1(2)
O2-Mn1-O3	91.03(8)	C23-N1-Mn1	112.9(2)

[a] Symmetry code i): $-x, 1-y, 1-z$.

the Mn_2 dimer through an almost linear two-center hydrogen bond. The distance between the O4 donor atom and the O2 acceptor atom is 2.826 Å and the O4-H4-O2 angle is 162.4°.

Since the two Mn centers are interrelated by a crystallographic inversion center, they have identical coordination geometries. The hexacoordinate Mn atoms have rather irregularly shaped coordination octahedra comprising the N_2O_4 donor set on each metal atom. The N1-Mn1-O1 angle (164.22°) shows that the axial ligand atoms are tilted away from the planar Mn_2O_2 moiety. Moreover, there is a significant difference in bond length between the axial Mn1−O1 (1.907 Å), Mn1−N1 (2.100 Å) pair and the equatorial Mn1−N2 (2.188 Å), Mn1−O3 (2.264 Å) pair. This geometrical distortion could be expected for an octahedral high-spin d^4 Mn^{III} ion. Therefore the Jahn–Teller axis is oriented along the N2−Mn1−O3 bonds in the Mn_2O_2 plane.

In **3a**, the Mn−Mn distance (3.3168 Å) is somewhat greater than other Mn^{III}−Mn^{III} contacts in $Mn_2(\mu$-OR$)_2$ systems.[31] This elongation can possibly be attributed to the combined effect of the Jahn–Teller axis and the well-defined geometrical restrictions imposed by the pentadentate ligand structure.[32, 33] Recently, the μ-phenoxide dimer [Mn^{III}(sa-
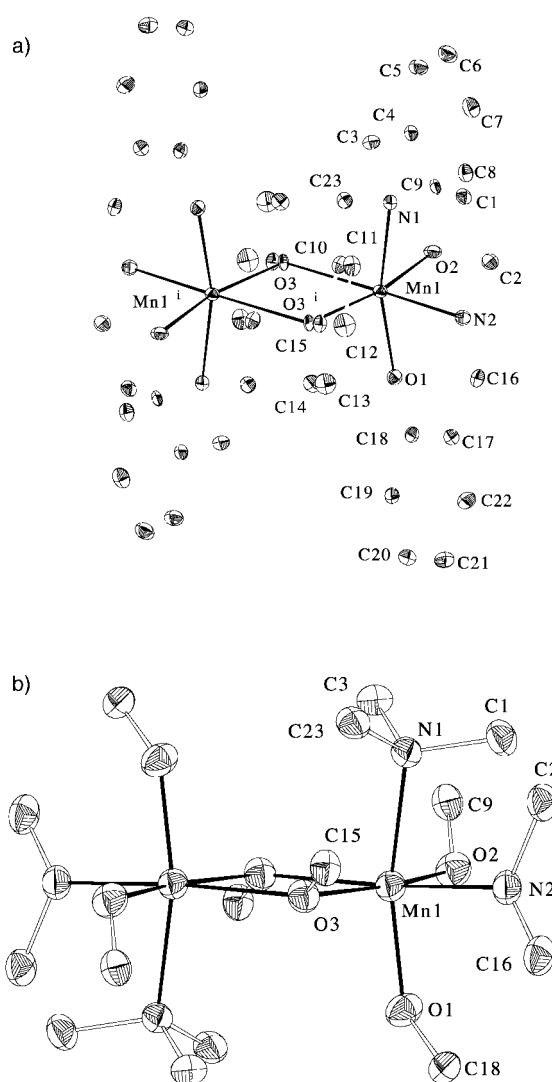
Figure 3. a) Structure of $[C_{23}H_{21}MnN_2O_3]_2 \cdot CH_3OH$ (**3a**) (ORTEP view; ellipsoids at 50% probability level; symmetry code: i) $-x, -y, -z$). b) Structure of $[C_{23}H_{21}MnN_2O_3]_2 \cdot CH_2Cl_2$ (**3b**) (ORTEP view; ellipsoids at 50% probability level; symmetry code: i) $1-x, 1-y, 1-z$).

len)(H_2O)]$_2$(H_2O)$_2$ was reported to have a comparable Mn−Mn distance (3.334 Å) and also an N_2O_4 coordination environment around each Mn atom.[15]

Some of the internal pentadentate ligand geometry has similiar features in the two complexes described here. As in the monomer **2**, C=N imine bonds (1.277 Å) are present in the dimeric complex **3a**.

Bond valence sums calculated from the X-ray diffraction structural parameters gave the very reasonable oxidation state of 2.92 for the Mn atoms.[28]

Crystal structure of **3b**: The molecular structure of **3b** (Figure 3b, Table 4) is very similar to that of **3a**. The main difference is the greater Mn···Mn distance (3.489 Å) in **3b**. The presence of a five-coordinate Mn^{III} complex in both solution and the solid state, together with its assembled dinuclear forms in the solid state, shows that Mn^{III} is capable of forming labile complexes on combination with the pentadentate ligand **1**. In addition, a potentially important feature

Table 4. Selected bond lengths [Å] and angles [°] for **3b**.[a]

Mn1−Mn1^i	3.348(9)	C4−C9	1.403(7)
Mn1−O2	1.892(4)	C5−C6	1.380(9)
Mn1−O1	1.928(3)	C6−C7	1.384(9)
Mn1−O3^i	1.934(4)	C7−C8	1.398(9)
Mn1−N1	2.119(4)	C8−C9	1.416(8)
Mn1−N2	2.193(4)	C10−C15	1.379(7)
Mn1−O3	2.284(3)	C10−C11	1.383(8)
O2−C9	1.347(6)	C10−C23	1.517(8)
O1−C18	1.344(6)	C11−C12	1.406(9)
O3−C15^i	1.380(6)	C12−C13	1.362(9)
O4−C24	1.401(5)	C13−C14^i	1.387(9)
N1−C3	1.488(7)	C15−C14^i	1.405(8)
N1−C1	1.496(6)	C16−C17	1.453(8)
N1−C23	1.530(6)	C17−C22	1.415(9)
N2−C16	1.284(7)	C17−C18	1.409(7)
N2−C2	1.462(7)	C18−C19	1.389(7)
C1−C2	1.509(8)	C19−C20	1.400(9)
C3−C4	1.516(8)	C20−C21	1.369(9)
C4−C5	1.412(8)	C21−C22	1.368(9)
O2-Mn1-O1	91.4(2)	C18-O1-Mn1	131.8(3)
O2-Mn1-O3^i	166.9(2)	C9-O2-Mn1	127.2(3)
O1-Mn1-O3^i	93.3(2)	C15^i-O3-Mn1^i	118.1(3)
O2-Mn1-N1	88.6(2)	C15^i-O3-Mn1	128.5(3)
O1-Mn1-N1	165.1(2)	Mn1-O3-Mn1^i	104.8(2)
O3^i-Mn1-N1	90.9(2)	C3-N1-C1	111.7(4)
O2-Mn1-N2	94.8(2)	C3-N1-C23	106.3(4)
O1-Mn1-N2	86.5(2)	C1-N1-C23	109.7(4)
O3^i-Mn1-N2	98.0(2)	C3-N1-Mn1	110.0(3)
N1-Mn1-N2	78.7(2)	C1-N1-Mn1	106.8(3)
O2-Mn1-O3	91.8(2)	C23-N1-Mn1	112.4(3)
O1-Mn1-O3	98.4(2)	C16-N2-C2	119.7(5)
O3-Mn1-O3^i	75.2(2)	C16-N2-Mn1	124.7(4)
N1-Mn1-O3	96.5(2)	C2-N2-Mn1	115.2(3)
N2-Mn1-O3	171.7(2)		

[a] Symmetry code i): $1 - x$, $1 - y$, $1 - z$.

of the mononuclear complex **2** is the vacant coordination site (Tables 1–4).

Magnetic studies: The magnetic susceptibility curves of **2** and **3** are different, but they are difficult to interpret, perhaps because of the presence of impurities such as ferromagnetic particles in the samples, as suggested by a referee.

Electrochemistry: Voltammograms of **2** in acetonitrile are shown in Figure 4 and the electrochemical data are summarized in Table 5. The differential pulse voltammogram (upper insert, Figure 4) shows two cathodic ($E_{pk} = -0.25$ V, -2.36 V) and three major anodic peaks ($E_{pk} = 0.55$ V, 1.20 V, 1.75 V).

The second reduction and the third oxidation occur at potentials at the limit of the potential range given by the background solvent. In cyclic voltammetry the first reduction gives a quasi-reversible wave at $E_{1/2} = -0.26$ V and the second reduction results in a wave at $E_{1/2} = -2.45$ V with a weak reverse peak. An irreversible wave with $E_{pa} = 0.60$ V corresponding to the first oxidation was observed at low sweep rate (10 mV s^{-1}), whereas faster scans (500 mV s^{-1}) resulted in a minor reverse peak at $E_{pc} = 0.46$ V. An ill-defined wave corresponding to the second oxidation was observed in slow scans (10 mV s^{-1}), whereas faster scans (500 mV s^{-1}) showed a well-defined but totally irreversible wave with $E_{pa} = 1.30$ V. The second oxidation process resulted in deposition of insoluble oxidation products on the working electrode,
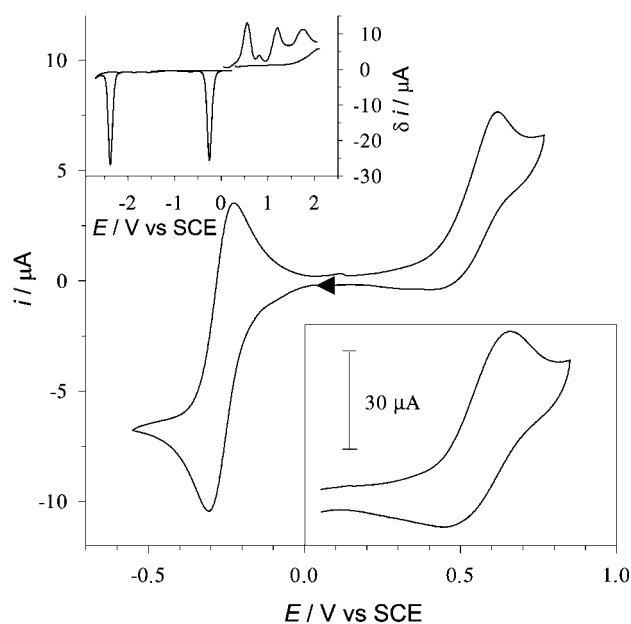
Figure 4. Cyclic voltammogram of complex **2** (2 mM) in CH$_3$CN (10 mV s^{-1}). Upper inset: Differential pulse voltammogram. Lower inset: Oxidative scan (500 mV s^{-1}).

Table 5. Electrochemical data for Mn^{III}L in CH$_3$CN solution with 0.1M [N(n-C$_4$H$_9$)$_4$]PF$_6$ as supporting electrolyte.

	2nd Reduction	1st Reduction	1st Oxidation	2nd Oxidation	3rd Oxidation
E_{pk}[a] [V]	− 2.36	− 0.25	0.55	1.20	1.75
$E_{1/2}$ [V][b]	− 2.37	− 0.26	0.53	–	–
ΔE_p [mV]	110[c], 80[c], 145[d]	190[d]	–	–	

[a] Differential pulse voltammetry peak potential. [b] ± 0.02 V. [c] 10 mV s^{-1}. [d] 500 mV s^{-1}.

necessitating polishing after each scan. According to the voltammetric peak heights all the electrode reactions can be assigned to one-electron processes, although the difference in degrees of reversibility makes an exact count uncertain. The one-electron nature of the first reduction and the first oxidation was confirmed coulometrically. No reliable coulometric measurements could be performed on either the second reduction or the second oxidation because of electrolyte reduction and deposition on the electrode, respectively.

Identical electrochemical behavior was observed for the different batches of the complex that had been characterized in the solid state as **2** or **3a**, respectively. Peak potentials, voltammetric peak currents and coulometric measurements were identical, within experimental error, for solutions with the same formal concentration of the monomeric unit, indicating that either **2** dimerizes in solution or, more probably, **3a** is solvolyzed to **2**. Dimerization in solution seems unlikely, considering the electrochemical results, since the metal-centered redox processes in a dimer can be expected to split considerably due to the coulombic interaction of the metal ions, rather than resulting in a single two-electron process.

Spectroelectrochemistry: The intense absorption at 300 nm ($\varepsilon_{247} = 22400$ dm^3 mol^{-1} cm^{-1}) in the electronic spectrum of **2**

in acetonitrile (Figure 5) is assigned to ligand-centered transitions by comparison with the spectrum of the ligand (not shown). The broad visible absorption of the complex can be assigned to charge transfter (CT) transitions, for example, phenolate to Mn^{III} ligand-to-metal charge transfers (LMCTs). Multiple LMCTs could arise from different ligand functions as well as from splitting of the metal states in a complex with reduced symmetry.
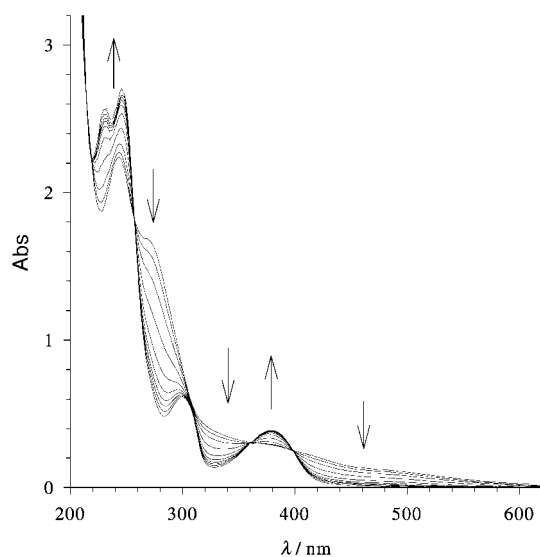
Figure 5. Electronic spectrum of complex **2** (1 mM) in CH_3CN and spectral changes upon electroreduction at -0.70 V.

Upon reduction of **2** to $[2]^-$(Figure 5) almost all visible absorption is lost, in agreement with the assignment to Mn^{III} LMCTs, and sharp isosbestic points at 215, 219, 257, 361, and 398 nm are observed in the course of the reduction. The increasing absorption at 380 nm ($\varepsilon_{380} = 3900 \ dm^3 mol^{-1} cm^{-1}$) is possibly due to a Mn^{II}-to-phenolate metal-to-ligand charge transfer (MLCT), and spectral changes below 300 nm might arise from the effect of the metal oxidation state on the ligand-centered (LC) transitions.

Upon the first oxidation an increasing absorption at all wavelengths above 300 nm was observed initally as indicated by the dashed arrows in Figure 6a, whereas only the LC transitions at 247 and 270 nm were losing intensity (not shown). After 120 s, however, absorption between 470 and 650 nm and below 370 nm began to decrease, while a further increase in absorption was observed between 360 and 470 nm and above 650 nm with reasonably sharp isosbestic points at these wavelengths that were maintained for 20 min. Comparison of the spectrum observed after 120 s with the spectrum of **2** showed the largest increases in absorption around 550 nm and below 350 nm. The difference spectrum obtained by subtracting the initial spectrum of **2** from the spectrum observed at 120 s (Figure 6b) can be assigned to the initial product transiently formed in the oxidation of **2** (solid line). The EPR spectra of the electro-oxidized complex suggest that a Mn^{IV} complex represents the initial oxidation product of **2**. The electronic spectrum supports this assignment since similar spectra have been observed with Mn^{IV}–phenolate complexes and have been assigned to the phenolate-to-Mn^{IV}
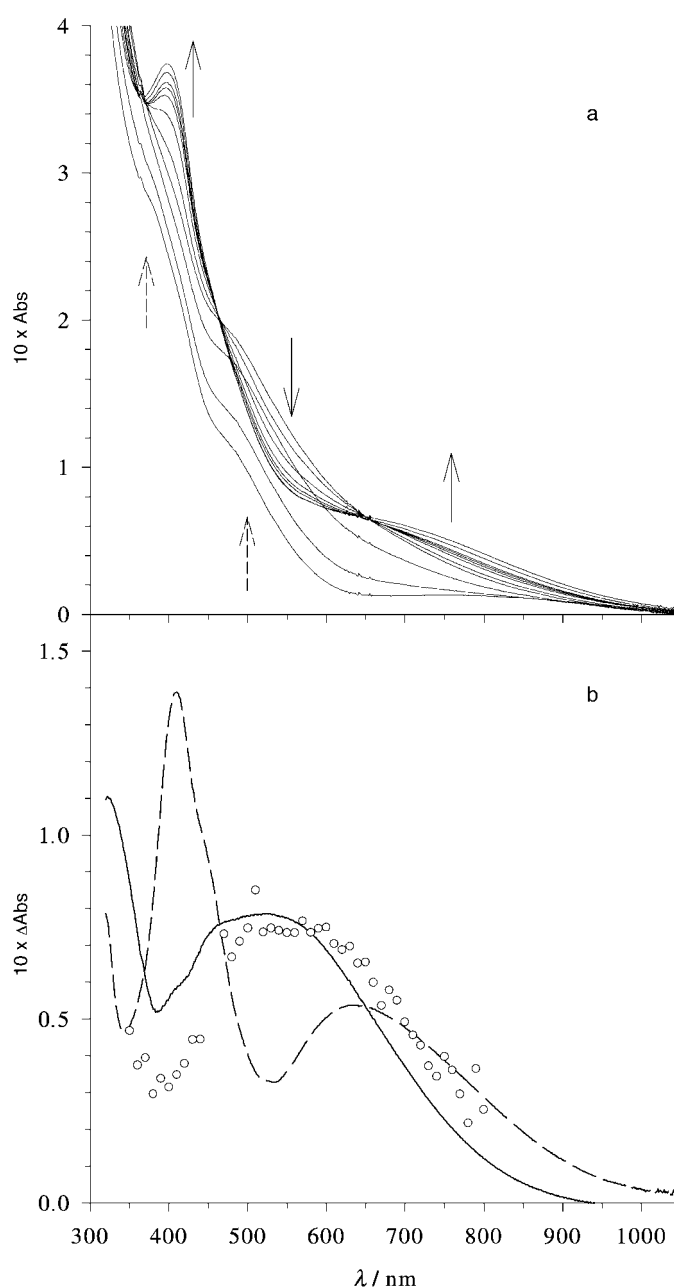
Figure 6. Electro- and photo-oxidation of complex **2** in CH_3CN: a) spectral changes upon electro-oxidation of complex **2** (1 mM) at 0.70 V from 0 to 120 s (dashed arrows) and 120 to 1200 s (solid arrows); b) normalized transient absorption spectrum ($\bigcirc$) observed by laser plash photolysis upon oxidation of complex **2** (0.3 mM) with photogenerated $Ru(bpy)_3^{3+}$ and difference spectra for electro-oxidation: spectrum at 120 s minus spectrum at 0 s (——) and spectrum at 1200 s minus spectrum at 0 s (– – –).

LMCTs.[16, 17, 19, 23] The product subsequently formed from $[2]^+$ showed two absorption bands peaking around 400 and 650 nm. The difference spectrum obtained by subtracting the initial spectrum of **2** from a spectrum observed after complete electro-oxidation at 0.70 V (after 1200 s; dashed line) consisted of a sharp band at 410 nm and a broad, less intense band with a maximum at 630 nm; these are well-known signatures of phenoxyl radicals.[34] A similar spectrum has been reported for the oxidation product of a Mn^{IV}–O–Mn^{III} dimer with a phenolate ligand and has been

attributed to a phenoxyl radical. The formation of a phenoxyl radical in this complex was evidenced by characteristic vibrational bands in the resonance Raman spectrum of the oxidized Mn^{IV} complex.[16] Thus, on the basis of the electronic spectrum the oxidation product subsequently formed by oxidation of **2** at 0.70 V can be identified as a phenoxyl radical. This is also suggested by EPR spectroscopy (see below). The coordination to the metal center seems to prevent the radical from fast bimolecular decay. This explains the unusual persistence of the radical at room temperature, which is well known for sterically hindered phenols.[35] A similar effect has been observed for other metal-coordinated or hydrogen-bonded radicals.[36–39] Since direct oxidation of phenolate does not occur at the potential of the first oxidation, we suggest that the phenoxyl radical is formed by catalytic oxidation of the phenolate group via the intermediate Mn^{IV} species [Eq. (2)]. The idea that the phenoxyl radical

$$[Mn^{IV}L]^+ \rightarrow [Mn^{III}L^\cdot]^+ \qquad (2)$$

is coordinated to Mn^{III} rather than to Mn^{IV} is supported by the one-electron nature of the first oxidation and the decay of the 530 nm band assigned to a phenolate-to-Mn^{IV} LMCT concomitantly with the formation of the phenoxyl radical.

To support the results of the spectroelectrochemical measurements that suggest that one-electron oxidation of **2** represents a metal-centered oxidation resulting initially in a Mn^{IV} species, we studied the oxidation of **2** on the time scale of laser flash photolysis. Photogenerated $[Ru(bpy)_3]^{3+}$ (bpy = 2,2′-bipyridine) was used as the one-electron oxidant ($E_{1/2}$ = 1.28 V). This complex was obtained from oxidative quenching of $[*Ru(bpy)_3]^{2+}$ with either methylviologen (4,4′-dimethylbipyridinium) or *p*-benzoquinone.[40] The reaction of **2** with $[Ru(bpy)_3]^{3+}$ proceeds with a bimolecular rate constant of 4 × 10^9 dm^{3}mol^{-1}s^{-1}. The spectrum of the product observed 10 μs after the excitation is shown in Figure 6b (open circles). The shape of the transient spectrum from flash photolysis is in reasonable agreement with the difference spectrum initially observed upon electro-oxidation (Figure 6b, solid line). In particular, it lacks the 400 nm band attributed to the phenoxyl radical that might already be present to some extent in the early spectrum shown in Figure 6b. If the spectral assignments based on the EPR results below, and similarities to reported UV/Vis spectra, are assumed to be correct, the results of the flash photolysis experiments provide further evidence that a Mn^{IV} species, rather than $[Mn^{III}L^\cdot]^+$, represents the initial oxidation product of **2**.

When complex **2** was oxidized at 1.30 V, an increasing absorption was observed over the whole visible spectrum, together with a bleaching of the absorption below 300 nm, but no isosbestic point survived the course of this interconversion. The magnitude of the spectral changes was approximately twice that of the change observed upon oxidation at 0.70 V. In contrast to the oxidation at 0.70 V, no intermediate increase in absorption around 500 nm, which can be attributed to a Mn^{IV} species, was observed.

In Figure 7, the final spectra after oxidation at 0.70 V (broken line) and 1.30 V (solid line) are compared after subtraction of the initial spectrum of **2**. The spectra are very
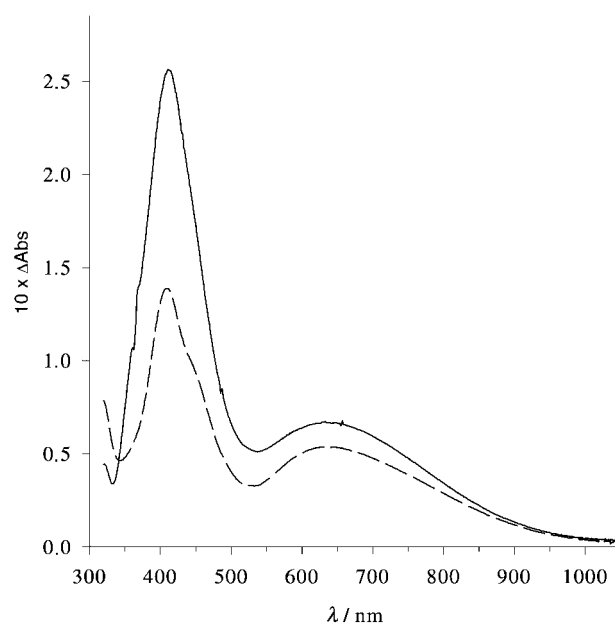
Figure 7. Electro-oxidation of complex **2** in CH$_3$CN: spectra at 1200 s minus spectra at 0 s for oxidation at 0.70 V (– – –) and 1.30 V (——).

similar and can be assigned to phenoxyl radicals, in agreement with the observation of a spin-coupled radical in the EPR spectrum (see below). Judging from the magnitude of the 410 nm band, oxidation at 1.30 V forms approximately twice as great a concentration of phenoxyl radicals as the oxidation at 0.70 V. The formation of more than one radical site on the complex seems unlikely and we suggest that oxidation at 1.30 V creates a higher concentration of the $[Mn^{III}L^\cdot]^+$ radical by direct oxidation of the ligand compared with the slower formation of $[Mn^{III}L^\cdot]^+$ via a Mn^{IV} species [Eq. (2)] that occurs at 0.70 V. Direct oxidation of the ligand at the higher potential is in agreement with the absence of absorption by a Mn^{IV} intermediate observed by spectroelectrochemistry during oxidation at 1.30 V, in contrast to the oxidation at 0.70 V. The $[2]^+$ observed by EPR spectroscopy at this potential (see below) is most probably due to the incomplete oxidation caused by deposition on the electrode under the bulk electrolysis conditions employed for EPR sample preparation. This problem affects the electrolysis in the spectroelectrochemical OTTLE (optically transparent thin layer electrochemical) cell less severely and allows for complete conversion of **2**, since a small amount of compound is electrolyzed at a relatively large electrode.

EPR spectroscopy: EPR spectra of the title compounds and their oxidation and reduction products have been recorded in frozen acetonitrile solution. The two batches, identified as **2** and **3a** in the solid state, displayed identical EPR properties in all the oxidation states investigated.

EPR spectroscopy was performed with the oscillating B_1 field of the microwave irradiation parallel to the static magnetic field in a dual-mode cavity. For complex **2**, a signal approximately 300 G wide was then observed, centered around $g = 8.1$ and displaying six well-resolved hyperfine lines, with a splitting of 45 G (Figure 8a), which is a signature
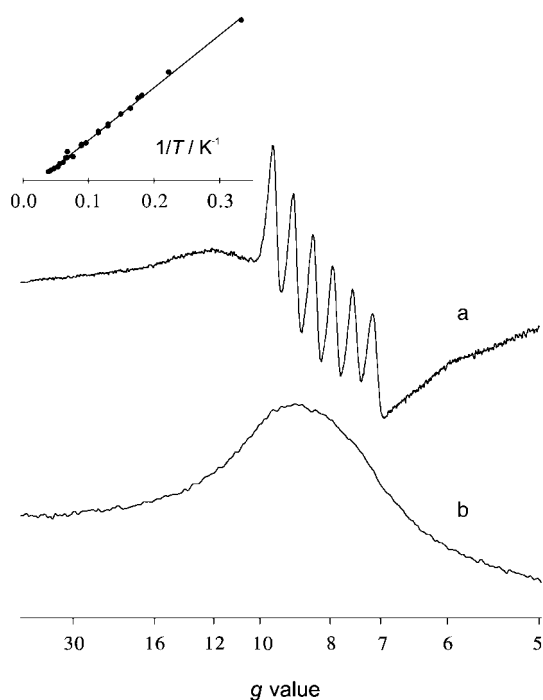
Figure 8. EPR spectra of complex **2**, dissolved in ethanol/methanol (50:50, v/v): a) polarization of the microwave B_1 field parallel to the external (B_0) field; b) polarization of B_1 perpendicular to B_0. The signal in a), centered around $g = 8$, displays six well-resolved hyperfine lines typical for a monomeric Mn^{III} complex with axial symmetry. Insert (top): signal amplitude of the Mn^{III} signal species in a) as a function of the reciprocal temperature. Spectrometer settings (microwave frequency, microwave power): a) 9.30 GHz, 32 mW; b) 9.60 GHz, 13 mW. Both spectra: modulation amplitude 10 G; temperature 4.2 K.

for a monomeric Mn^{III} species.[41] The temperature dependence of the signal intensity obeys the Curie law (Figure 8, insert), which indicates a negative value for the zero-field splitting parameter D (not shown). Similar parallel-mode EPR signals have been observed previously in Mn superoxide dismutase, Photosystem II and several inorganic Mn^{III} compounds.[41, 42, 43] In these previous studies, the signals were simulated and explained as arising from transitions between the $M_s = \pm 2$ levels in an $S = 2$ state of a Mn^{III} ion. Campbell et al. showed that the splitting between the six hyperfine lines from a Mn^{III} species varies according to the ligand environment, and depends on the zero-field splitting parameters D and E, that is, the coordination geometry.[43] The geometry for a Mn^{III} ion with a negative value for the axial parameter D can be either six-coordinate and tetragonally elongated, or a five-coordinate square pyramid. It has been suggested[43] that a relatively small hyperfine splitting constant $A_{\parallel}$, such as the 45 G splitting in the present case, can be best accounted for by a five-coordinate square pyramid. The crystal structure data of **2** revealed that the Mn^{III} ion is five-coordinate, and has a geometry that might be regarded as distorted square-pyramidal. Therefore, the EPR properties of **2**, in the light of the crystal data, support the predictions made by Campbell et al.[43]

Apart from the resolved hyperfine structure, the EPR spectrum of **2** also displays an underlying structureless feature, about 700 G wide. The unstructured signal is centered

at a slightly higher g value, about $g = 9$. In the traditional perpendicular mode the spectrum displayed a distinctive peak at $g = 8.5$ (Figure 8b). Somewhat similar EPR signals have been reported for dinuclear $Mn^{III/IV}$ complexes.[41] However, both Campbell et al. and Bryliakov et al. recently reported perpendicular-mode EPR signals from monomeric Mn^{III}–salen complexes, very similar to the one in Figure 8b.[44, 45] The results suggest that it is mainly the monomeric **2** that is observed in the EPR spectra, but the presence of dimer **3a** in the frozen solutions studied by EPR spectroscopy cannot be excluded.

The first reversible reduction can be assigned to a metal-centered process resulting in $[\mathbf{2}]^-$, as suggested by the EPR spectra observed after electrolysis at -0.50 V. The intensity of the EPR spectrum of **2** decreased to about 6 % of the starting amplitude (not shown). In the traditional perpendicular EPR mode, two spectroscopic species were then observed, of which only one was visible at 4 K. It is a broad and complex spectrum at low field, with a maximum around $g = 5$ (Figure 9a). It displayed a number of lines with partly resolved fine structure, approximately 80 G apart. With increasing temperature, the signal amplitude decreased and at 10 K a different spectrum became visible (Figure 9a, peaks beween approximately 2500 and 4500 G.). It is several kilogauss
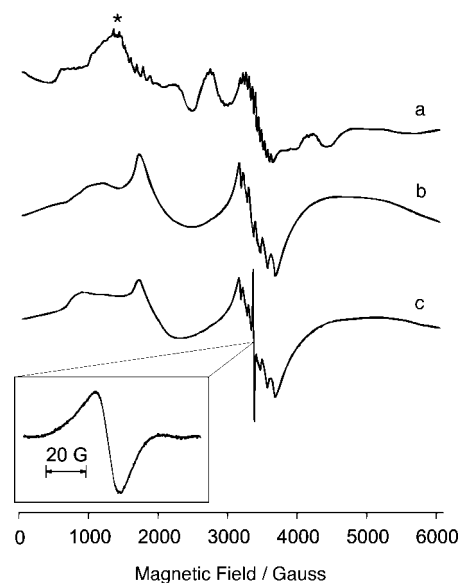
Figure 9. EPR spectra of complex **2** in perpendicular polarization, after bulk electrolysis at different electrode potentials (see Results section). a) After reduction by one electron per complex. The signal species marked with an asterisk possibly originates from the lowest lying doublet in a monomeric Mn^{II} species with large zero-field splittings. The spectral features at higher magnetic field are from excited integer spin states in a coupled $Mn_2^{II,II}$ dimer. b) After oxidation by one electron per complex. The peak at $g = 4$ is a typical feature of a Mn^{IV} compound ($S = 3/2$). The structured signal species at $g = 2$ is likely to originate from Mn^{II} in a symmetrical environment, that has been released from its original ligand environment after the oxidation. c) After oxidation by two electrons per complex, followed by a quick transfer to a sample tube and freezing in liquid nitrogen. Apart from the spectral features in b), an organic radical is observed at $g = 2.032$ (see also insert). The radical is likely to be associated with the ligand molecule, and near (a few ångströms from) a metal ion (see text). Spectrometer settings: temperature, in a) and insert, 20 K, and in b), c), 4 K; microwave power 13 mW (insert, 6 mW); microwave frequency 9.60 GHz; modulation amplitude 10 G.

broad, and has the characteristics of a weakly ferromagnetically coupled Mn^{II}/Mn^{II} dimer, in an excited spin state with $S \neq 0$. Comparable spectra from coupled Mn^{II}/Mn^{II} dimers have been reported on several occasions and are well characterized.[46] The origin of the first species, observed at low temperature, is unclear. In low-symmetry Mn^{II} centers, the zero-field splitting causes the levels in the spin system to be nondegenerate and often only the lowest-lying doublet can be observed. Broad resonances with a variety of structures, with g values ranging from 5 to 8, have been observed in cases of low-symmetry centers in Mn^{II} compounds, as well as in some Mn enzymes.[47] The signal at $g = 5$ probably arises from a monomeric Mn^{II} complex in a distorted geometry. The second species, visible from 10 K to about 50 K, is clearly a coupled Mn^{II}/Mn^{II} dimer. The coulometric analysis showed that one electron per Mn ion had been transferred and it is very unlikely that the reduction of both metal centers in a coupled dimer would occur at the same potential as a two-electron process. In addition, it should be possible to detect formation of a Mn^{II}/Mn^{III} dimer. Therefore, it has to be assumed that the Mn^{II}/Mn^{II} dimer has been formed upon one-electron reduction of **2** to **[2]**$^-$ and subsequent dimerization. Since voltammetry shows only one reversible peak for the re-oxidation of **[2]**$^-$ to **2**, the dimerization seems to occur only as the temperature is decreased to form the rigid solvent employed in the EPR experiments.

Re-oxidation at 0.05 V afforded about 80% of the initial **2**, (as evidenced by coulometry and EPR spectroscopy), indicating limited long-term stability of **[2]**$^-$.

Electrolysis at 0.70 V resulted in the formation of a Mn^{IV} complex together with free Mn^{II} ions as indicated by the observation of two distinct peaks in the EPR spectra. The first gives rise to a sharp peak with $g = 4$, accompanied by a broad, unresolved resonance around $g = 5–6$ (Figure 9b). The peak at $g = 4$ is the signature of a monomeric Mn^{IV} ion in an axial $S = 3/2$ configuration, which is expected from a one-electron oxidation of a monomeric Mn^{III} complex.[48] The $g = 6$ signal may be an additional feature of the Mn^{IV} spectrum.

A signal 600 G wide at $g = 2$ with six hyperfine lines was also observed. Although some Mn^{IV} compounds have been shown to display similar EPR signals, it is more likely that the $g = 2$ signal in our case arises from Mn^{II} ions, apparently released from the ligand since further oxidation of the complex resulted in an increase in the $g = 2$ signal but rendered the $g = 4$ signal unchanged (see below).[49] Integration of the signal and comparison with a standard sample gave an estimated concentration of Mn^{II} of 60 μM, or 6% of the total amount of **2** in the sample. Oxidation of the ligand that could account for the release of free Mn^{II} ions is likely to occur at a potential similar to the potential of the Mn^{III}–Mn^{IV} couple as apparent from the voltammograms of the complex and of the protonated ligand (not shown). According to the EPR spectra, the relative concentration of the Mn^{IV} complex, compared with that of free Mn^{II}, is higher in a partly oxidized sample (0.4 charge equivalents) taken after 40 s of electrolysis than after exhaustive electrolysis (6–8 min). This shows that the Mn^{IV} complex represents a short-lived intermediate of the first oxidation. Together with the results of spectroelectrochemistry and laser flash photolysis experiments (see above)

this suggests that the oxidation of the ligand proceeds via the initial formation of **[2]**$^+$.

According to the EPR spectra, no **2** was recovered by re-reduction of the oxidized sample at 0.05 V and the fraction (approimately 10% of one charge equivalent) that passed during electrolysis has to be assigned to processes other than re-reduction of **[2]**$^+$ to **2**.

Further oxidation at 1.40 V of a sample first oxidized at 0.70 V did not result in formation of additional **[2]**$^+$ or in higher oxidation states of manganese, but gave rise to an increase in the EPR signal from free Mn^{II} (90 μM).

Electrolysis of a solution of **2** at 1.40 V, aiming for rapid, sequential two-electron oxidation, gave only 40% of the expected two-electron charge equivalent before the current had decayed almost completely, mainly because of deposition on the electrode. The EPR spectrum of this solution again displayed the Mn^{IV} and Mn^{II} signals, but the Mn^{II} formed was only about 40 μM. In addition to these previously observed signals, a radical signal at $g = 2.03$, peak-to-trough width 15 G, also appeared (Figure 9, insert). The radical signal was not saturated at microwave powers up to 20 mW, which indicates that it is close, and magnetically coupled, to a metal center, although probably not coordinated to it. The absence of fine structure in the signal makes confirmation of the chemical identity of the radical difficult. However, according to its electronic spectrum obtained by spectroelectrochemistry, it can be identified as a phenoxyl radical.

Conclusion

By reaction of the trisphenolate ligand **1** with Mn^{III}, a pentacoordinate complex **2** could be isolated. On crystallization from methanol or dichloromethane, the dimers **3a** and **3b** could also be isolated. A combination of electrochemistry and EPR spectroscopy showed that, in acetonitrile, this complex was mainly monomeric, perhaps because the solvent coordinated to the sixth position. However, the mononuclear complex **2** was probably in equilibrium with the dimer **3** and perhaps also with complexes of higher nuclearity, as suggested by the detection of both the trimer and the tetramer by electrospray ionization mass spectrometry (ESI-MS).

It is clear that high manganese oxidation states, Mn^{IV} or Mn^V, are required for oxidation of water. Attempts to observe a Mn^V–oxo species formed by reaction of **2** with iodosobenzene have been unsuccessful so far, but the successful use of **2** as epoxidation catalyst shows that such species can be formed, although they are probably short-lived[45, 50] (see also H. Schmitt, unpublished results). This is also suggested by the EPR studies of the species formed by electrochemical oxidation of **2**. Upon one-electron oxidation, a Mn^{IV} species was formed, which was at least partly converted to another species, containing a loosely coordinated phenoxy radical. Attempted conversion of these species to Mn^V seemed to result in over-oxidation of the ligand, as indicated by EPR signals which probably stemmed from Mn^{II}. Catalytic formation of oxygen via a Mn^V–oxo complex thus seems difficult, but may still be possible if the reaction is fast enough, in analogy with the epoxidation which does work. However, it is

probable that ligands that are less readily oxidized than simple phenols will be required for the formation of an efficient catalyst.

Experimental Section

Syntheses

N,N′-Bis(2-hydroxybenzyl)-1,2-diaminoethane: This was prepared essentially as described previously.[51] Salicylaldehyde (10.45 mL, 100 mmol) was added to a stirred solution of ethylenediamine (3.34 mL, 50 mmol) in ethanol (150 mL). Immediately the solution turned yellow and within a minute a yellow precipitate was formed. The mixture was refluxed for 1 h, during which the yellow compound redissolved, and then it was cooled to 0 °C. The regained precipitate was filtered off and a second crop was collected by evaporation followed by resuspension in small amounts of ice-cold ethanol and filtering. The solid was washed with small amounts of ice-cold ethanol and dried in air to give yellow flakes (13.06 g, 48.7 mmol; 98 % yield). ^{1}H NMR (300 MHz, CDCl$_3$, 25 °C, TMS): $\delta = 3.95$ (s, 4H), 6.85 (t, 2H), 6.90 (d, 2H), 7.20 (d, 2H), 7.30 (t, 2H), 8.35 ppm (s, 2H).

This product (5.14 g, 19.2 mmol) was suspended in stirred methanol (100 mL) and sodium borohydride (1.465 g, 38.36 mmol) was added in small portions. Gas evolution was observed and after 0.5 h the suspension was colorless. The mixture was cooled and the crystals that formed were isolated by filtration and washed with cold methanol to afford *N,N′*-bis(2-hydroxybenzyl)-1,2-diaminoethane (3.9 g, 14 mmol; 75 % yield) as a white powder. ^{1}H NMR (300 MHz, CDCl$_3$, 25 °C, TMS): $\delta = 2.85$ (s, 4H), 4.00 (s, 4H), 6.80 (t, 2H), 6.85 (d, 2H), 7.00 (d, 2H), 7.20 ppm (t, 2H).

N,N,N′-Tris(2-hydroxybenzyl)-1,2-diaminoethane (1): *N,N′*-Bis(2-hydroxybenzyl)-1,2-diaminoethane (3.79 g, 13.9 mmol) was suspended in stirred methanol (80 mL) and salicylaldehyde (1.46 mL, 14.0 mmol) was added, causing a yellow coloration. After refluxing for 1 h a clear solution was obtained. Evaporation of the solvent gave a yellow-white precipitate which was suspended in *n*-hexane (100 mL) and boiled. Cooling and filtration (washing with *n*-hexane) gave a yellow-white powder (4.88 g, 13.0 mmol; 93 % yield).[32] ^{1}H NMR (300 MHz, CDCl$_3$, 25 °C, TMS): $\delta = 2.70$ (d t, 2H), 3.30 (d t, 2H), 3.40 (d, 2H), 4.00 (s, 1H), 4.10 (d, 2H), 6.80 (m, 3H), 6.90 (t, 1H), 6.95 (d, 1H), 7.05 (d, 2H), 7.15 (m, 3H), 7.30 ppm (t, 2H).

This compound (2.00 g, 5.32 mmol) was suspended in stirred methanol (30 mL), and trichloroacetic acid (0.906 g, 5.32 mmol) was added. When everything had dissolved, the solution was cooled to -78 °C and sodium borohydride (0.329 g, 8.61 mmol) was added in small portions. After 5 h, the temperature was slowly raised to room temperature and the mixture was stirred overnight. The precipitate was isolated by filtration, washed with a small amount of cold methanol, and dried to give **1** (1.49 g, 3.94 mmol; 74 % yield) as a white powder. ^{1}H NMR (300 MHz, CDCl$_3$, 25 °C, TMS): $\delta = 2.70$ (t, 2H), 2.90 (t, 2H), 3.70 (s, 4H), 3.80 (s, 2H), 6.70 – 7.15 ppm (m, 12H); ^{13}C NMR (100 MHz, CDCl$_3$, 25 °C): $\delta = 44.9$, 49.6, 51.6, 54.05, 115.3, 118.4, 118.6, 123.2, 124.1, 127.8, 128.3, 128.6, 130.0, 156.5, 156.9 ppm; MS: *m/z* 379 $[M+\mathrm{H}]^+$.

Complexation with manganese(III)

Preparation of 2: A mixture of *N,N,N′*-tris(2-hydroxyphenylmethyl)ethylenediamine (**1**) (0.151 g, 0.4 mmol), Mn(ClO$_4$)$_3$ · 6 H$_2$O (0.325 g, 0.8 mmol) and NaOAc (0.098 g, 1.2 mmol) was dissolved in acetone/water (5:1, v/v). A dark solution was obtained, which was stirred for 15 min, then left overnight. The manganese complex **2** was obtained as a dark crystalline solid (0.156 g, 0.35 mmol, 87 % yield). Crystallization from methanol and water gave crystals suitable for X-ray analysis. Elemental analysis (%) calcd for C$_{23}$H$_{21}$MnN$_2$O$_3$(H$_2$O): C 61.9, H 5.15, Mn 12.3, N 6.3, O 14.3; found: C 62.1, H 5.32, Mn 12.35, N 6.1, O 14.1.

Preparation of 3a: By the same procedure as for **2**, but using two equivalents of Mn(OAc)$_3$, the crude complex **3a** was obtained. Recrystallization from methanol gave dark crystals of **3a**, which were suitable for X-ray analysis.

Preparation of 3b: Mn(OAc)$_3$ (1.300 g, 4.849 mmol) was suspended in stirred methanol (75 mL). Ligand **1** (0.601 g, 1.590 mmol) in dichloromethane (75 mL) was added and the mixture was refluxed for 1 h. The reaction mixture was washed with water (3 × 100 mL), dried with sodium

sulfate, filtered, and evaporated to give a black powder (0.235 g, 0.549 mmol, 34.5 % yield), which was a mixture of **2** and **3**. IR spectroscopy showed the presence of an imine group. The crude complex was characterized by cyclic voltammetry and EPR spectroscopy. ESI-MS showed strong peaks at *m/z* 429.791 $[M+\mathrm{H}]^+$, 489.874 $[M+\mathrm{HOAc}+\mathrm{H}]^+$, and 858.107 $[(M)_2+\mathrm{H}]^+$. Minor peaks appeared at 808.158 and 1286.146 $[(M)_3+\mathrm{H}]^+$. At high senstivity, a peak at 1714.726, corresponding to the tetramer, could also be observed along with many other peaks, which were not assigned.

Crystals of **3b** were obtained by dissolving the crude product in dichloromethane, then slowly evaporating the solvent to give thin dark flakes, which were suitable for X-ray analysis.

X-ray crystal structures: Suitable single crystals of C$_{23}$H$_{21}$MnN$_2$O$_3$ (**2**), [C$_{23}$H$_{21}$MnN$_2$O$_3$]$_2$ · CH$_3$OH (**3a**), and [C$_{23}$H$_{21}$MnN$_2$O$_3$]$_2$ · CH$_2$Cl$_2$ (**3b**) were selected and mounted on glass fibers with epoxy glue. The data for **2, 3a**, and **3b** were collected on a Stoe image-plate diffractometer at $T = 293$, 110, and 293 K, respectively. Unit cell dimensions: **2**: $a = 13.6483(15)$, $b = 7.1591(8)$, $c = 19.831(2)$ Å, $\beta = 97.828(13)°$, $V = 1919.6(4)$ Å^3; **3a**: $a = 10.0688(9)$, $b = 16.7667(17)$, $c = 12.6703(12)$ Å, $\beta = 98.523(11)°$, $V = 2115.4(3)$ Å^3; **3b**: $a = 10.133(2)$, $b = 11.135(2)$, $c = 12.548(2)$ Å, $\alpha = 117.72(2)$, $\beta = 98.523(11)$, $\gamma = 96.31(2)°$, $V = 1171.8(4)$ Å^3. Intensity data were corrected for absorption effects using the X-SHAPE program package.[52] Systematic absences in the diffraction data were consistent with space group *P*2$_1$/*n* (no. 14) for both **2** and **3a**. Additional crystallographic data are given in Table 1. The structure of **2** was solved by conventional heavy-atom techniques, and of **3a** and **3b** by direct methods (SHELXS-97).[53] All three structures were refined by full-matrix least-squares on F^2 (SHELXL97).[54] The R values are defined as $R(\mathrm{int}) = \Sigma |F_o^2 - F_o^2(\mathrm{mean})| / \Sigma[F_o^2]$, $S = [\Sigma[w(F_o^2 - F_c^2)^2]/(n-p)]^{1/2}$, $R_1 = \Sigma ||F_o| - |F_c|| / |F_o|$, $wR_2 = [\Sigma[w(F_o^2 - F_c^2)^2]/\Sigma[w(F_o^2)^2]]^{1/2}$. CCDC-166458 (**2**), CCDC-166459 (**3a**), and CCDC-166460 (**3b**) contain the supplementary crystallographic data for this paper. These data can be obtained free of charge via www.ccdc.can.ac.uk/conts/retrieving.html (or from the Cambridge Crystallographic Centre, 12 Union Road, Cambridge CB21EZ, UK; Fax: (+44) 1223-336033; or deposit@ccdc.cam.ac.uk).

Magnetic susceptibility measurements: Preliminary magnetic susceptibilities were measured for both complexes. The AC magnetic susceptibilities on powdered polycrystalline samples of **2** and **3a** were measured (500 Hz and 1000 A m^{-1}) in the range 11 – 320 K with a Lake Shore Inc. AC Susceptometer, Model 7130, equipped with a helium cryostat. Diamagnetic corrections were made using Pascal's constants.[55]

Electrochemistry: Cyclic voltammetry, differential pulse voltammetry, and controlled potential electrolysis were performed by using a three-electrode system connected to an Autolab potentiostat with a GPES electrochemical interface (Eco Chemie). The working electrode was a glassy carbon disc (diameter 2 mm, freshly polished) for voltammetry or a platinum grid cylinder (15 mm × 15 mm diameter) for bulk electrolysis. A platinum spiral in a compartment separated from the bulk solution by a fritted disk was used as counter electrode. The reference electrode was a nonaqueous Ag/Ag$^+$ electrode (CH Instruments, 10 mM AgNO$_3$ in acetonitrile) in a separate compartment with a potential of -0.08 V versus the ferrocene/ferrocenium couple in acetonitrile as an external standard. All potentials are reported relative to the saturated calomel electrode (SCE); they were converted by adding 0.30 V to the potentials measured against the Ag/Ag$^+$ electrode according to $E_{1/2} = 0.38$ V versus SCE for the ferrocene/ferrocenium couple.[56]

Electrolyte solution was prepared from dry acetonitrile (Merck, spectroscopy grade, dried with MS 3 Å) with 0.1 M tetrabutylammonium hexafluorophosphate (TBAPF$_6$, Fluka, electrochemical grade) that had been dried at 373 K. The glassware was oven-dried, assembled and flushed with argon while hot. Before all measurements oxygen was removed by bubbling the stirred solutions for 10 min with solvent-saturated argon and the samples were kept under an argon atmosphere during measurement.

The EPR samples were prepared electrochemically by bulk electrolysis of 2 – 5 mL solutions of the Mn complex (1 mM) at controlled potentials. After electrolysis 250 µL samples were transferred to argon-flushed EPR tubes, frozen immediately and kept in liquid nitrogen.

UV/Vis spectroelectrochemistry: Spectroelectrochemical measurements were made in an OTTLE-type quartz cell, optical path length 1 mm. A

10 mm × 30 mm platinum grid (400 mesh per cm^2) was used as working electrode. The counter and reference electrodes were as described in the Electrochemistry section above.

Solvent-saturated argon was bubbled into the samples for 20 min and they were then transferred with the argon current to the argon-flushed cell. The spectra were recorded on a UV/Vis diode array spectrophotometer (Hewlett Packard 8435).

EPR spectroscopy: EPR measurements were performed on a Bruker E500 X-band spectrometer equipped with a dual-mode cavity and an Oxford Instruments ESR900 flow cryostat. Complexes **1a** and **2a** were dissolved to 1 mM in dry acetonitrile and frozen in liquid nitrogen before measurements. Spectrometer settings were modulation frequency 100 kHz, modulation amplitude 10 G; all spectra were taken at 4 K. See the figure legends for further details.

Flash photolysis: Flash photolysis measurements with optical transient absorption detection were performed with a laser flash photolysis set-up consisting of a Nd:YAG laser/OPO combination (Quantel) and a flash photolysis spectrometer (Applied Photophysics). The samples were excited at 460 nm with an energy of 30 mJ per 5 ns pulse. Mn^{III}L (0.1 – 1 mM) was disolved in acetonitrile (Merck, spectroscopy grade) containing Ru(bpy)$_3$(PF$_6$)$_2$ ($\approx 40\,\mu$M, Abs$_{460}$ = 0.6) and methylviologen hexafluorophosphate (20 mM) or p-benzoquinone (10 mM, Fluka, $\geq 99.5\%$). The bimolecular rate constant of the reaction of Mn^{III}L with [Ru(bpy)$_3$]$^{3+}$ was determined from a pseudo first-order plot of the recovery rate for [Ru(bpy)$_3$]$^{2+}$ observed at 450 nm with methylviologen as quencher. To avoid the intense and broad absorption of the reduced methylviologen, transient spectra were recorded with p-benzoquinone as acceptor. Oxygen was removed by bubbling with solvent-saturated nitrogen.

Acknowledgements

[1] B. A. Diner, G. T. Babcock, *Oxygenic Photosynthesis: The Light Reactions* (Eds.: D. Ort, C. F. Youcum), Kluwer, The Netherlands, **1996**, pp. 213 – 247.

[2] R. D. Britt, *Oxygenic Photosynthesis: The Light Reactions* (Eds.: D. R. Ort, C. F. Youcum), Kluwer, The Netherlands, **1996**, pp. 137 – 164.

[3] J. Barber, W. Kuhlbrandt, *Curr. Opin. Struct. Biol.* **1999**, *9*, 469.

[4] V. K. Yachandra, K. Sauer, M. P. Klein, *Chem. Rev.* **1996**, *96*, 2927 – 2950.

[5] W. Ruttinger, G. C. Dismukes, *Chem. Rev.* **1997**, *97*, 1 – 24.

[6] P. E. M. Siegbahn, R. H. J. Crabtree, *J. Am. Chem. Soc.* **1999**, *121*, 117 – 127.

[7] J. Limburg, J. S. Vrettos, H. Chen, J. de Paula, R. H. J. Crabtree, G. W. Brudvig, *J. Am. Chem. Soc.* **2001**, *123*, 423 – 430.

[8] E. N. Jacobsen, *Catalytic Asymmetric Synthesis* (Ed.: I. Ojima), VCH, New York **1993**, p. 159.

[9] T. Katsuki, *Coord. Chem. Rev.* **1995**, *140*, 189 – 214.

[10] T.Katsuki, *J. Mol. Catal. A: Chem.* **1996**, *113*, 87.

[11] C. T. Dalton, V. M. Ryan, V. M. Wall, C. Bousquet, D. G. Gilheany, *Top. Catal.* **1998**, *5*, 75 – 91.

[12] J. T. Groves, J. Lee, S. S. Marla, *J. Am. Chem. Soc.* **1997**, *119*, 6269 – 6273.

[13] C. G. Miller, S. W. Gordon-Wylie, C. P. Horwitz, S. A.Strazisar, D. K. Peraino, G. R. Clark, S. T. Weintraub, T. J. Collins, *J. Am. Chem. Soc.* **1998**, *120*, 11540 – 11541.

[14] T. J. Collins, *Acc. Chem. Res.* **1994**, *27*, 279 – 285.

[15] M. J. Baldwin, T. L. Stemmler, P. J. Riggs-Gelasco, M. L. Kirk, J. E. Penner-Hahn, V. L. Pecoraro, *J. Am. Chem. Soc.* **1994**, *116*, 11349 – 11356.

[16] O. Horner, E. Anxolabehrere-Mallart, M.-F. Charlot, L. Tchertanov, J. Guilheim, T. A. Mattioli, A. Boussac, J J Girerd, *Inorg. Chem.* **1999**, *38*, 1222 – 1232.

[17] S. K. Chandra, A. Chakravorty, *Inorg. Chem.* **1992**, *31*, 760 – 765.

[18] S. K. Chandra, P.Basu, D. Ray, S. Pal, A. Chakravorty, *Inorg. Chem.* **1990**, *29*, 2423 – 2428.

[19] D. P. Kessissoglou, X. Li, W. M. Butler, V. L. Pecoraro, *Inorg. Chem.*, **1987**, *26*, 2487 – 2492.

[20] A. Böttcher, H. Elias, E. G. Jäger, H. Langfelderova, M. Mazur, L. Muller, H. Paulus, P. Pelikan, M. Rudolf, M. Valko, *Inorg. Chem.* **1993**, *32*, 4131 – 4138.

[21] A. W. Addison, T. N. Rao, J. Reedijk, J. van Rijn, G. C. Verschoor, *J. Chem. Soc. Dalton Trans.* **1984**, 1349 – 1356.

[22] Y.-M. Frapart, A. Boussac, R. Albach, R. E. Anxolabehere-Mallart, M. Delrosse, J.-B. Verlhac, G. Blondin, J.-J. Girerd, J. Guilhem, M. Cesario, A. W. Rutherford, D. Lexa, *J. Am. Chem. Soc.* **1996**, *118* , 2669 – 2678.

[23] A. Neves, S. Erthal, I. Vencato, A. S. Ceccato, Y. P. Mascarenhas, O. R. Nascimento, M. Hörner, A. A. Batista, *Inorg. Chem.* **1992**, *31*, 4749 – 4755.

[24] P. A. Goodson, J. Glerup, D. J. Hodgson, K. Michelsen, E. Pedersen, *Inorg. Chem.* **1990**, *29*, 503 – 508.

[25] P. A. Goodson, A. R. Oki, J. Glerup, D. J. Hodgson, *J. Am. Chem. Soc.* **1990**, *112*, 6248 – 6254.

[26] P. A. Goodson, J. Glerup, D. J. Hodgson, K. Michelsen, H. Weihe, *Inorg. Chem.* **1991**, *30*, 4909 – 4914.

[27] J. Glerup, P. A. Goodson, A. Hazell, R. Hazell, D. J. Hodgson, C. J. McKenzie, K. Mickelsen, Y. Rychlewska, H. Toftlund, *Inorg. Chem.* **1994**, *33*, 4105 – 4111.

[28] M. O'Keeffe, N. E. Brese, *J. Am. Chem. Soc.* **1991**, *113*, 3226 – 3229.

[29] Y. Ciringh, S. W. Gordon-Wylie, R. E. Norman, G. R. Clark, S. T. Weintraub, C. P. Horwitz, *Inorg. Chem.* **1997**, *36*, 4968 – 4975.

[30] X. Li, V. L. Pecoraro, *Inorg. Chem.* 1989, *28*, 3403 – 3410.

[31] N. A. Law, M. T. Caudle, V. L. Pecoraro, *Adv. Inorg. Chem.* **1999**,*46*, 305 – 440.

[32] H.-L. Shyu, H.-H. Wei, Y. Wang, *Inorg. Chim. Acta* **1999**, *290*, 8 – 13.

[33] S. Gou, Q. Zeng, Z. Yu, M. Qian, J. Zhu, C. Duan, X. You, *Inorg. Chim. Acta* **2000**, *303*, 175 – 180.

[34] E. R. Altwickler, *Chem. Rev.* **1967**, *67*, 475 – 531.

[35] V. V. Pavlishchuk, A. W. Addison, *Inorg. Chim. Acta* **2000**, *298*, 97 – 102.

[36] J. Müller, A. Kikuchi, E. Bill, T. Weyhermüller, P. Hildebrandt, L. Ould-Moussa, K. Wieghardt, *Inorg. Chim. Acta* **2000**, *297*, 265 – 277.

[37] F. N. Penkert, T. Weyhermüller, E. Bill, P. Hildebrandt, S. Lecomte, K. Wieghardt, *J. Am. Chem. Soc.* **2000**, *122*, 9663 – 9673.

[38] T. Maki, Y. Araki, Y. Ishida, O. Onomura, Y. Matsumura, *J. Am. Chem. Soc.* **2001**, *123*, 3371 – 3372.

[39] L. Sun, M. Burkitt, M. Tamm, M. K. Raymond, M. Abrahamson, D. LeGourriérec, Y. Frapart, A. Magnuson, P. Huang Kenéz, P. Brandt, A. Tran, L. Hammarström, S. Styring, B. Åkermark, *J. Am. Chem. Soc.* **1999**, *121*, 6834 – 6842.

[40] K.Kalyanasundaraman, *Photochemistry of Polypyridine and Porphyrin Complexes,* Academic Press, London, **1992**, pp. 157 – 161.

[41] D. P. Goldberg, J. Telser, J. Krzystek, A. G. Montalban, L.-C. Brunel, A. G. M. Barrett, B. M. Hoffman, *J. Am. Chem. Soc.* **1997**, *119*, 8722 – 8723.

[42] R. D. Britt, J. M. Peloquin, K. A. Campbell, *Annu. Rev. Biophys. Biochem.* **2000**, *29*, 463 – 495.

[43] K. A. Campbell, E. Yikilmaz, C. V. Grant, W. Gregor, A.-F. Miller, R. D. Britt, *J. Am. Chem. Soc.* **1999**, *121*, 4714 – 4715.

[44] K. P. Bryliakov, D. E. Babushkin, E. P. Talsi, *Mendeleev Commun.* **1999**, *1*, 29 – 32.

[45] K. A. Campbell, M. R. Lashley, J. K. Wyatt, M. H. Nantz, R. D. Britt, *J. Am. Chem. Soc.* **2001**, *123*, 5710 – 5719.

[46] H. Diril, H. R. Chang, M. J. Nilges, X. Zhang, J. A. Potenza, H. J. Schugar, S. S. Isied, D. N.Hendrickson, *J. Am. Chem. Soc.* **1989**, *111*, 5102 – 5114.

[47] G. H. Reed, G. D. Markham, *Biological Magnetic Resonance, Vol. 6* (Eds: L. J. Berliner, J. Reuben), Plenum Press, New York, **1984**, pp. 73 – 142.

[48] K. R. Rodgers, H. M. Goff, *J. Am. Chem. Soc.* **1988**, *110*, 7049 – 7060.

[49] S. Pal, P. Ghosh, A. Chakravorty, *Inorg. Chem.* **1985**, *24*, 3704 – 3706.

B. Åkermark et al.

[50] W. Adam, C. Mock-Knoblauch, C. R. Saha-Möller, M. Herdrich, *J. Am. Chem. Soc.* **2000**, *122*, 9685 – 9691.

[51] J. H. Billman, L. Dorman, C. Linneaus, *J. Med. Chem.* **1963**, *6*, 701 – 705.

[52] STOE, X-SHAPE, revision 1.09, Crystal Optimisation For Numerical Absorption Correction, Darmstadt, Germany, **1997**.

[53] G. M. Sheldrick, SHELXL-97, Program for the Refinement of Crystal Structures, University of Göttingen, Göttingen (Germany), **1997**.

[54] G. M. Sheldrick, *Acta Crystallogr. Sect. A* **1990**, *46*, 467 – 473.

[55] H. Lueken, *Magnetochemie*, Teubner, Leipzig, **1999**, pp. 426 – 427.

[56] V. V. Pavlishchuk, A. W. Addison, *Inorg. Chim. Acta* **2000**, 298, 97 – 102.

0947-6539/02/0816-3768 $ 20.00+.50/0